Electronic Supplementary Material (ESI) for Inorganic Chemistry Frontiers.

Electronic Supplementary Information

Lanthanide phosphonates with pseudo-D_{5h} local symmetry exhibiting magnetic and luminescence bifunctional properties

Min Ren,[a] Song-Song Bao,[a] Bing-Wu Wang,[b] Rute A. S. Ferreira,[c] Li-Min Zheng,[*a] Luis D. Carlos[*c]

[a]State Key Laboratory of Coordination Chemistry, School ofChemistry and Chemical Engineering, Collaborative Innovation Center of Advanced Microstructures, Nanjing University, Nanjing 210093, China

[b]Beijing National Laboratory for Molecular Sciences, State Key Laboratory of Rare Earth Materials Chemistry and Applications, College of Chemistry and Molecular Engineering, Peking University, Beijing 100871, P. R. China

[c]Physics Department, CICECO, University of Aveiro, 3810-193, Aveiro, Portugal

Table S1. Geometry analysis of **1–2** by SHAPE software

Compound	Pentagonal bipyramid (D_{5h})	Capped octahedron (C_{3v})	Capped trigonal prism (C_{2v})
1	1.76190	3.61921	2.50926
1	1.78176	3.66342	2.52627

Table S2. CF Parameters determined for compounds **1** and **2**.

Parameters	B_0^2 / cm^{-1}	B_0^4 / cm^{-1}	B_0^6 / cm^{-1}	SQX[a]
1	728(8)	-1492(3)	166(6)	0.0056
2	578(7)	-1715(8)	-641(6)	0.0081

a $SQX = \sqrt{\sum_{i=1}^{n} \left(\left[\chi_{obs}(i) - \chi_{calc}(i) \right] / \chi_{obs}(i) \right)^2}$

Table S3. Energies and corresponding composition of the 8 doublets of the $^6H_{15/2}$ multiplets calculated with the CF parameters for compound **1**. Contributions lower than 1% are not shown here.

	M_J sublevel	Energy / cm^{-1}
1	0.705 |±13/2> + 0.295 |±3/2>	0
2	0.909 |±11/2> + 0.091 |±1/2>	11.99
3	0.976 |±9/2> + 0.094 |±1/2>	104.9
4	|±15/2>	176.3
5	0.904 |±7/2> + 0.094 |±3/2>	227.4
6	|±5/2>	346.1
7	0.904|±3/2> + 0.058 |±7/2>+ 0.038 |±13/2>	437.6
8	0.871|±1/2> + 0.102|±9/2> + 0.019|±7/2>	486.9

Table S4. Energies and corresponding composition of the 8 doublets and 1 singlet of the $^5I_8$ multiplets calculated with the CF parameters for compound **2**. Contributions lower than 1% are not shown here.

	M_J stark sublevel	Energy / cm^{-1}
1	0.538|±7> + 0.212|±3/2>	0
2	0.538|±6> + 0.462|±2>	20.07
3	0.849|±5> + 0.143|±1>	142.0
4	0.736 |±4> + 0.264 |0>	251.0
5[a]	0.284 |+4> + 0.433 |0>+ 0.284 |-4>	286.2
6	0.732|±1> + 0.185|±3> +0.070 |±5>	294.4
7	0.447 |±3> + 0.179 |±7> +0.370 |±1>	304.5
8	0.874 |±2> + 0.117 |±6>	309.2
9	|±8>	371.9

a: this sublevel is singlet.

Table S5. The parameters obtained by fitting the *ac* magnetic susceptibilities of compound **1** in indicated *dc* field at 2 K.

H / kOe	χ_T/ cm^3·mol^{-1}	χ_S/ cm^3·mol^{-1}	ln(τ_A / s)	α_A	ln(τ_B / s)	α_B	f_A	R[a]
0.1	5.99(4)	5.64(6)	-7.58(1)	0.20(2)				6.8×10^{-6}
0.3	5.90(1)	3.90(4)	-7.36(1)	0.22(5)				8.8×10^{-5}
0.5	5.96(8)	2.63(4)	-7.05(7)	0.14(1)	-3.11(7)	0.16(2)	0.83(2)	8.8×10^{-6}
1.0	5.56(9)	0.82(1)	-6.19(1)	0.33(2)	-2.86(5)	0.03(1)	0.75(4)	6.5×10^{-5}
1.5	5.21(7)	0.28(8)	-6.00(1)	0.35(5)	-2.49(3)	0.05(1)	0.57(2)	3.3×10^{-4}
2.0	4.82(9)	0.13(2)	-6.26(5)	0.34(6)	-2.23(2)	0.09(2)	0.42(2)	1.0×10^{-3}
2.5	4.35(9)	0.11(1)	-6.69(5)	0.29(2)	-1.97(1)	0.09(3)	0.31(2)	1.0×10^{-3}
3.0	4.00(4)	0.06(4)	-7.24(5)	0.32(7)	-1.65(5)	0.14(4)	0.25(1)	2.2×10^{-3}

$$R = \sum\left[(\chi'_{obs}-\chi'_{cal})^2 + (\chi''_{obs}-\chi''_{cal})^2\right] / \sum\left[\chi'^{\,2}_{obs} + \chi''^{\,2}_{obs}\right]$$

Table S6. Summary of the parameters of relaxation A obtained by fitting the *ac* magnetic data of compounds **1** and **1a**.

compound	H / kOe	τ[a] / ms	A[b] / s^{-1}·K^{-1}·T^{-2}	B_1[b] / s^{-1}	B_2[b] / T^{-2}	C[c] / s^{-1}·K^{-9}	U_{eff} / K	τ_0 / s
1	1.5	2.48(2)	$5.6(4)\times10^3$	$2.5(6)\times10^3$	$6(2)\times10^3$	0[d]	41.6±1.3	$1.3(3)\times10^{-9}$
1	0.5	0.87(6)	$5.6(4)\times10^3$	$2.5(6)\times10^3$	$6(2)\times10^3$	0.17±0.04	39.9±1.1	$9.0(9)\times10^{-10}$
1a	1.5	6.46(13)	$3.2(3)\times10^3$	$1.5(3)\times10^3$	$2.4(9)\times10^3$	0[d]	36.9±1.8	$7.6(5)\times10^{-10}$

[a] obtained at 2 K; [b] Determined by fitting the H-dependence of τ; [c] parameter for Raman exponent (n = 9); [d] fixed to zero.

Table S7. The parameters obtained by fitting the *ac* magnetic susceptibilities of compound **1** under 0.5 kOe *dc* field.

T / K	χ_T/ cm^3·mol^{-1}	χ_S/ cm^3·mol^{-1}	ln(τ_A / s)	α_A	ln(τ_B / s)	α_B	f_A	R[a]
1.8	6.51(5)	2.94(2)	-6.46(2)	0.12(4)	-2.97(1)	0.12(3)	0.81(2)	1.3×10^{-5}
2.0	5.96(8)	2.63(4)	-7.05(3)	0.14(1)	-3.11(3)	0.16(3)	0.83(4)	8.9×10^{-6}
2.3	5.29(7)	2.27(8)	-7.75(4)	0.18(4)	-3.32(3)	0.16(3)	0.87(1)	5.9×10^{-6}
2.5	4.92(9)	2.10(2)	-8.13(2)	0.18(1)	-3.44(2)	0.20(3)	0.89(3)	5.8×10^{-6}
2.7	4.59(8)	1.97(4)	-8.45(1)	0.18(3)	-3.58(2)	0.22(2)	0.91(2)	8.0×10^{-6}
3.0	4.19(1)	1.84(6)	-8.90(2)	0.15(2)	-3.83(4)	0.36(5)	0.91(1)	1.3×10^{-5}
3.2	3.95(3)	1.72(3)	-9.25(2)	0.14(3)	-4.04(1)	0.37(3)	0.92(2)	8.6×10^{-6}
3.4	3.67(2)	1.54(7)	-9.77(5)	0.22(3)				9.5×10^{-5}
3.6	3.49(3)	1.05(1)	-10.30	0.26(1)				5.9×10^{-5}
3.8	3.33(3)	1.81(5)	-11.02	0.32(2)				4.4×10^{-5}

[a] $R = \sum\left[(\chi'_{obs}-\chi'_{cal})^2 + (\chi''_{obs}-\chi''_{cal})^2\right] / \sum\left[\chi'^{\,2}_{obs} + \chi''^{\,2}_{obs}\right]$

Table S8. The parameters obtained by fitting the *ac* magnetic susceptibilities of compound **1** under 1.5 kOe *dc* field.

T / K	χ_T/ cm^3·mol^{-1}	χ_S/ cm^3·mol^{-1}	ln(τ_A / s)	α_A	ln(τ_B / s)	α_B	f_A	R[a]
1.8	5.85(1)	0.38(4)	-5.87(2)	0.27(1)	-2.21(4)	0.08(1)	0.48(2)	6.4×10^{-5}
2.0	5.21(3)	0.28(2)	-6.00(1)	0.35(5)	-2.49(2)	0.05(4)	0.57(2)	3.3×10^{-4}
2.3	5.00(2)	0.23(1)	-6.21(1)	0.39(1)	-2.70(1)	0.13(2)	0.61(2)	8.8×10^{-5}
2.5	4.62(2)	0.21(4)	-6.15(4)	0.41(3)	-2.78(4)	0.04(3)	0.74(1)	1.9×10^{-4}
2.7	4.41(1)	0.22(1)	-6.46(2)	0.39(4)	-2.86(1)	0.19(4)	0.75(4)	6.9×10^{-5}
3.0	4.05(2)	0.23(2)	-7.08(4)	0.36(2)	-2.84(1)	0.17(3)	0.80(4)	8.9×10^{-5}
3.2	3.93(2)	0.33(1)	-7.81(3)	0.26(1)	-3.43(4)	0.40(4)	0.67(2)	2.1×10^{-4}
3.4	3.66(1)	0.44(3)	-8.37(1)	0.18(1)	-4.01(3)	0.41(1)	0.67(5)	2.9×10^{-5}
3.6	3.49(1)	0.45(4)	-8.95(3)	0.15(4)	-4.00(3)	0.41(3)	0.70(2)	1.0×10^{-4}
3.8	3.30(3)	0.55(2)	-9.46(4)	0.10(4)	-4.38(2)	0.42(2)	0.71(2)	2.0×10^{-5}
4.0	3.14(3)	0.53(5)	-10.03(2)	0.09(4)	-4.50(1)	0.41(4)	0.75(4)	2.8×10^{-5}

[a] $R = \sum\left[(\chi'_{obs}-\chi'_{cal})^2 + (\chi''_{obs}-\chi''_{cal})^2\right] / \sum\left[\chi'^{\,2}_{obs} + \chi''^{\,2}_{obs}\right]$

Table S9. The parameters obtained by fitting the *ac* magnetic susceptibilities of compound **1a** in indicated *dc* field at 2 K.

H / kOe	χ_T/ cm^3·mol^{-1}	χ_S/ cm^3·mol^{-1}	ln(τ_A / s)	α_A	R[a]
0.1	4.74(4)	3.16(4)	-7.16(3)	0.24(4)	1.6×10^{-5}
0.3	4.80(1)	1.08(2)	-5.99(1)	0.29(2)	1.0×10^{-4}
0.5	4.78(2)	0.52(1)	-5.47(1)	0.29(1)	2.1×10^{-4}
1.0	4.49(1)	0.27(5)	-5.08(1)	0.27(1)	4.4×10^{-4}
1.5	4.20(1)	0.20(3)	-5.04(2)	0.25(3)	7.2×10^{-4}
2.0	3.66(1)	0.15(2)	-5.39(2)	0.24(3)	6.9×10^{-4}
2.5	2.88(3)	0.17(1)	-6.02(2)	0.17(2)	4.9×10^{-4}
3.0	2.38(1)	0.16(4)	-6.56(5)	0.16(1)	8.3×10^{-4}

[a] $R = \sum\left[(\chi'_{obs}-\chi'_{cal})^2 + (\chi''_{obs}-\chi''_{cal})^2\right] / \sum\left[\chi'^{\,2}_{obs} + \chi''^{\,2}_{obs}\right]$

Table S10. The parameters obtained by fitting the *ac* magnetic susceptibilities of compound **1a** under 1.5 kOe *dc* field.

T / K	χ_T/ cm^3·mol^{-1}	χ_S/ cm^3·mol^{-1}	ln(τ_A / s)	α_A	R[a]
1.8	4.47(2)	0.17(3)	-4.64(2)	0.25(5)	4.2×10^{-4}
2.0	4.20(1)	0.20(4)	-5.04(2)	0.25(4)	7.1×10^{-4}
2.3	3.69(4)	0.26(1)	-5.99(1)	0.25(2)	3.7×10^{-4}
2.5	3.43(1)	0.31(3)	-6.80(4)	0.25(4)	3.6×10^{-4}
2.7	3.22(3)	0.31(2)	-7.72(2)	0.27(4)	3.0×10^{-4}
2.8	3.11(2)	0.30(5)	-8.21(1)	0.28(5)	4.8×10^{-4}

3.0	2.94(1)	0.32(5)	-9.22(4)	0.33(3)	2.0×10^{-4}
3.2	2.80(1)	0.31(3)	-10.41(4)	0.41(3)	1.7×10^{-4}
3.4	2.67(1)	0.31(3)	-12.31(1)	0.57(5)	1.7×10^{-4}

Table S11. The parameters obtained by fitting the *ac* magnetic susceptibilities of compound **2** in indicated *dc* field at 1.8 K.

H / kOe	χ_T/ $cm^3\cdot mol^{-1}$	χ_S/ $cm^3\cdot mol^{-1}$	$\ln(\tau / s)$	α	R^a
0.5	7.93(4)	2.43(1)	-14.77(1)	0.43(5)	9.3×10^{-7}
1.0	6.91(3)	2.43(1)	-12.32(1)	0.34(1)	2.0×10^{-6}
1.5	5.64(3)	2.43(2)	-11.46(1)	0.33(1)	2.3×10^{-6}
2.0	4.43(3)	1.60(1)	-11.40(1)	0.32(2)	6.8×10^{-6}
2.5	3.44(1)	0.95(1)	-11.42(3)	0.31(2)	1.4×10^{-5}
3.0	2.68(2)	0.43(1)	-11.44(4)	0.29(1)	5.1×10^{-6}

a $R = \sum\left[(\chi'_{obs}-\chi'_{cal})^2 + (\chi''_{obs}-\chi''_{cal})^2\right] / \sum\left[\chi'^{\,2}_{obs} + \chi''^{\,2}_{obs}\right]$

Table S12. The parameters obtained by fitting the *ac* magnetic susceptibilities of compound **2** under 1.5 kOe *dc* field.

T / K	χ_T/ $cm^3\cdot mol^{-1}$	χ_S/ $cm^3\cdot mol^{-1}$	$\ln(\tau / s)$	α	R^a
1.8	5.64(2)	2.43(1)	-11.46(1)	0.33(1)	2.3×10^{-6}
1.9	5.49(2)	2.50(1)	-11.47(2)	0.33(2)	2.3×10^{-6}
2.0	5.31(2)	2.40(1)	-11.46(3)	0.30(2)	1.1×10^{-5}
2.1	5.16(3)	2.49(5)	-11.47(3)	0.31(1)	1.6×10^{-6}
2.2	5.02(3)	2.45(1)	-11.52(5)	0.31(1)	1.0×10^{-6}
2.3	4.88(4)	2.43(4)	-11.58(1)	0.31(3)	8.0×10^{-6}
2.4	4.76(1)	2.20(1)	-11.75(4)	0.31(3)	1.1×10^{-6}
2.5	4.65(3)	2.29(3)	-11.80(1)	0.33(1)	7.4×10^{-7}
2.6	4.53(2)	2.10(1)	-11.89(2)	0.32(5)	1.7×10^{-6}
2.7	4.43(3)	2.10(1)	-11.93(1)	0.31(4)	9.5×10^{-7}
2.8	4.33(3)	2.20(1)	-12.06(3)	0.35(3)	4.9×10^{-6}
2.9	4.23(1)	2.10(1)	-12.10(3)	0.33(3)	2.1×10^{-6}
3.0	4.33(4)	2.10(1)	-12.15(1)	0.36(5)	4.9×10^{-6}
3.1	4.04(4)	2.10(1)	-12.24(2)	0.34(2)	1.2×10^{-6}

a $R = \sum\left[(\chi'_{obs}-\chi'_{cal})^2 + (\chi''_{obs}-\chi''_{cal})^2\right] / \sum\left[\chi'^{\,2}_{obs} + \chi''^{\,2}_{obs}\right]$

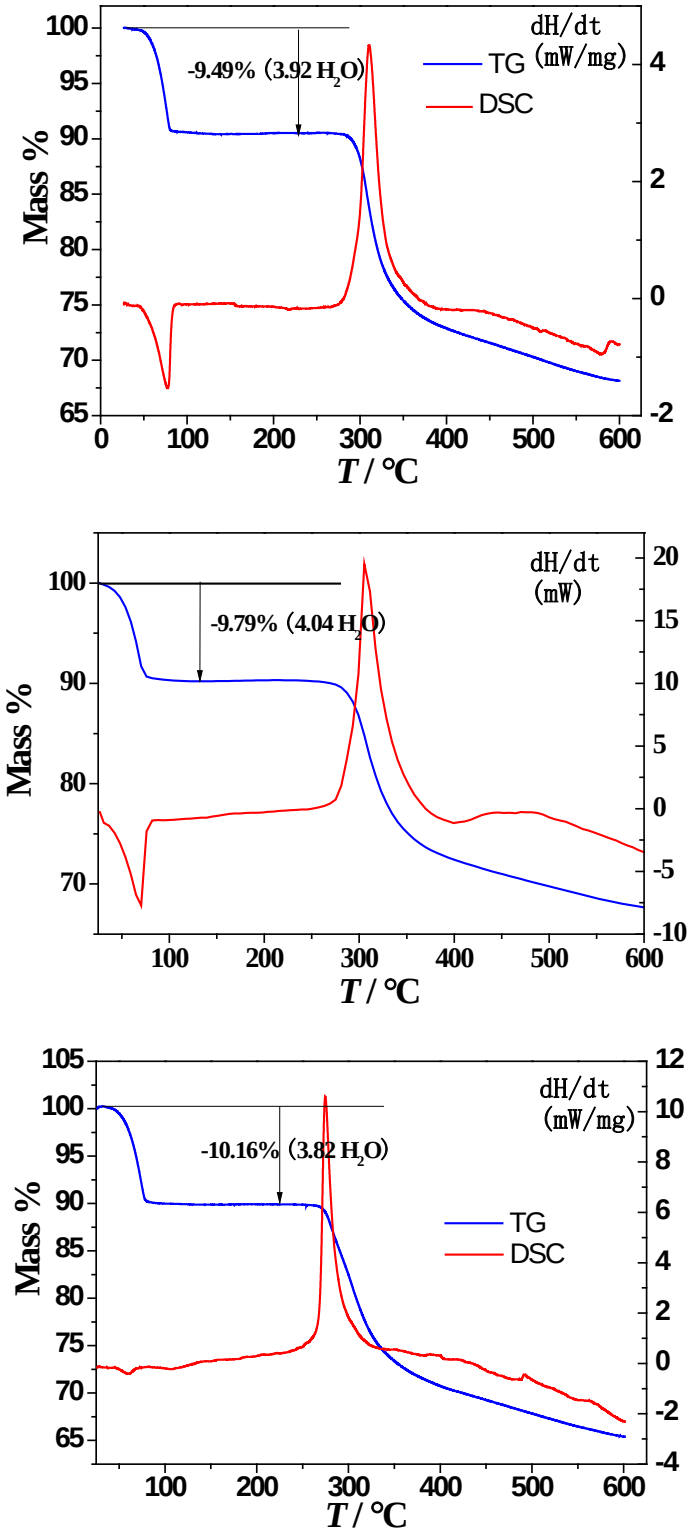

Figure S1. TG curves of compounds **1** (top), **2** (middle) and **1a** (bottom).

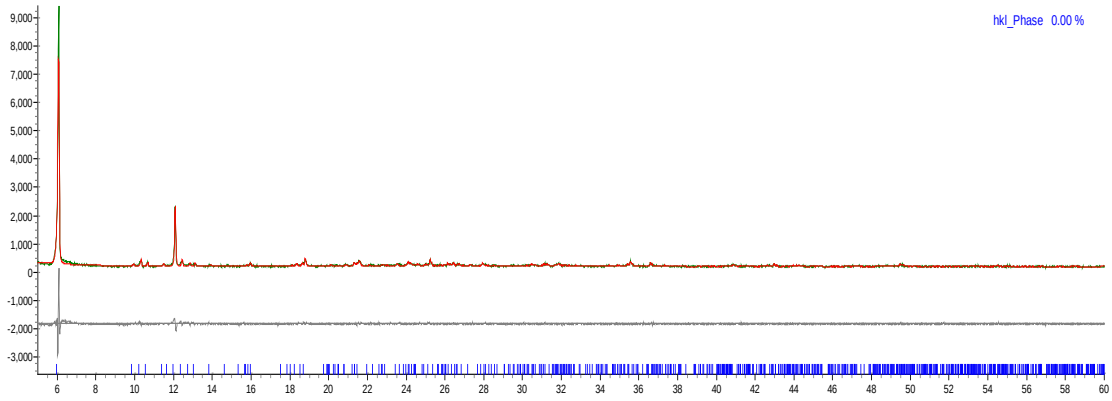

Figure S2. PXRD pattern of **1** refined by *TOPAS* software. *Rwp* = 8.78%. Cell parameters: *P*-1, a = 9.184 Å, b = 9.274 Å, c = 15.196 Å , α = 88.052 °, β = 76.383 °, γ = 75.812 °, V = 1218.7 $Å^3$

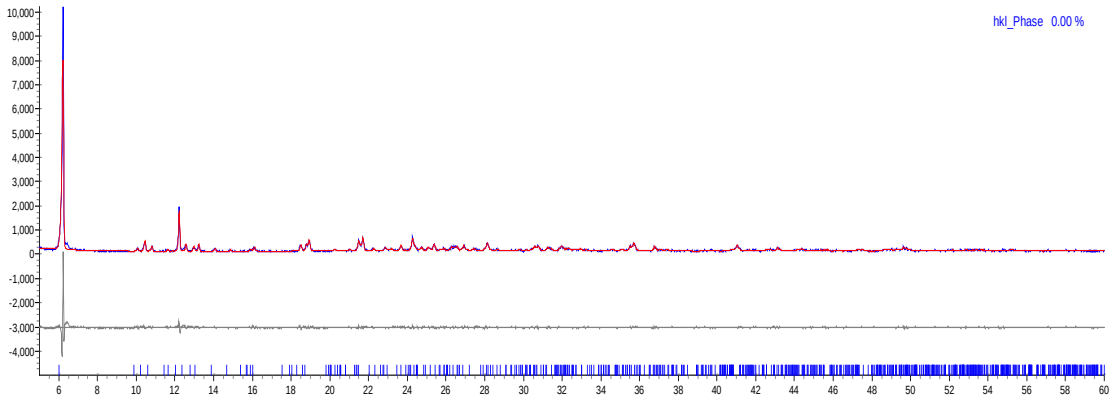

Figure S3. PXRD pattern of **2** refined by *TOPAS* software. *Rwp* = 11.72%. Cell parameters: *P*-1, a = 9.167 Å, b = 9.253 Å, c = 15.161 Å , α = 87.967 °, β = 76.471 °, γ = 75.754 °, V = 1211.5 $Å^3$

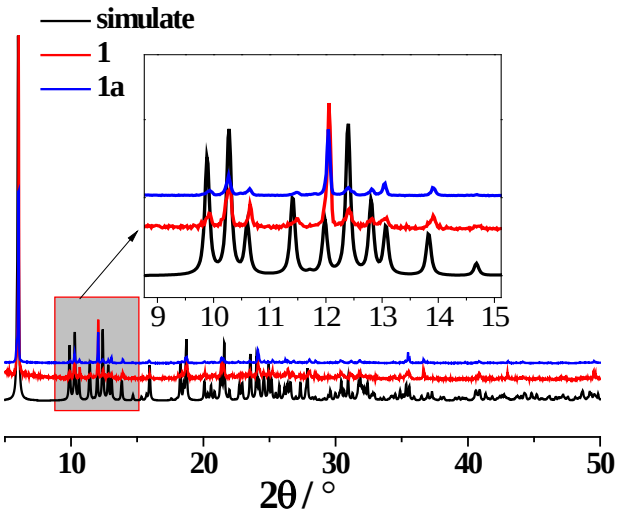

Figure S4. PXRD patterns for compounds **1** and **1a**, and that simulated from the single crystal data of **1**.

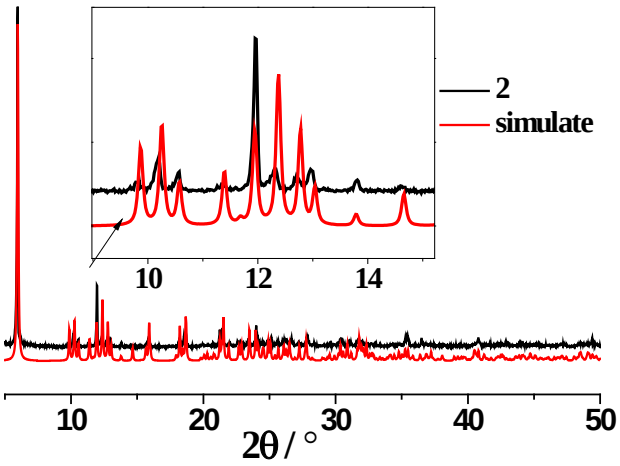

Figure S5. PXRD pattern for compound **2**, and that simulated from the single crystal data of **2**.

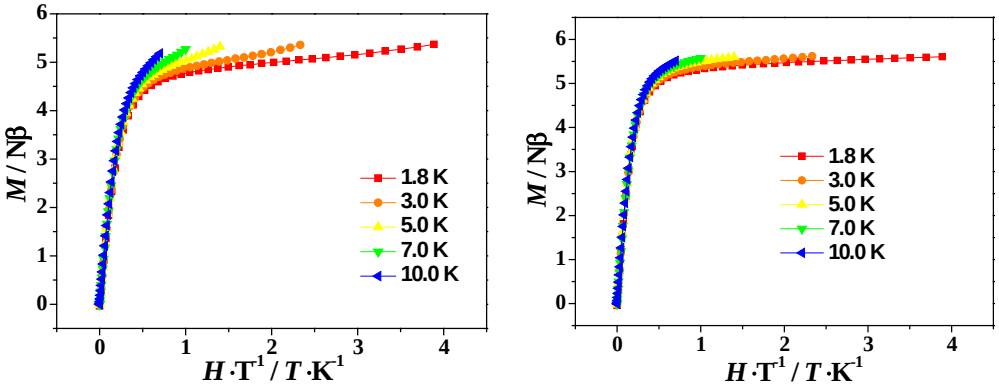

Figure S6. The *M vs. H/T* plots for **1** (left) and **2** (right) at the indicated temperatures

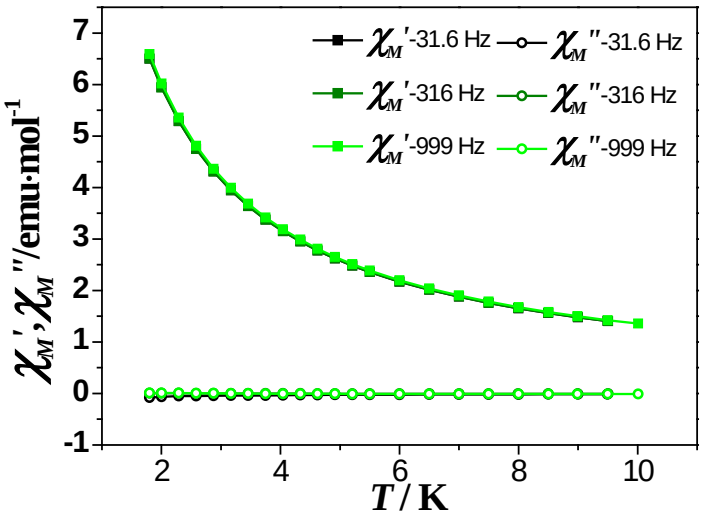

Figure S7. Temperature dependent in-phase (χ_M') and out-of-phase (χ_M") signals of **1** in zero *dc* field.

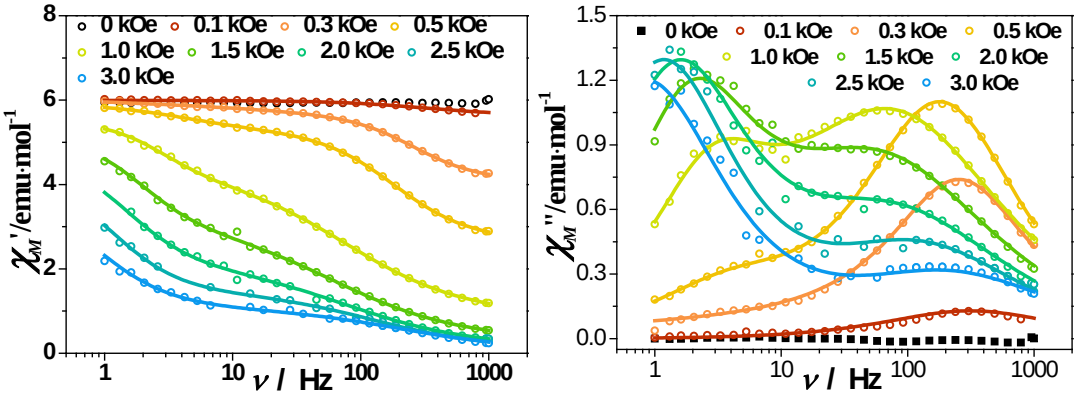

Figure S8. Frequency dependent in-phase (χ_M') and out-of-phase (χ_M") signals of **1** in indicated *dc* fields at 2 K. The solid lines represent the simulated results.

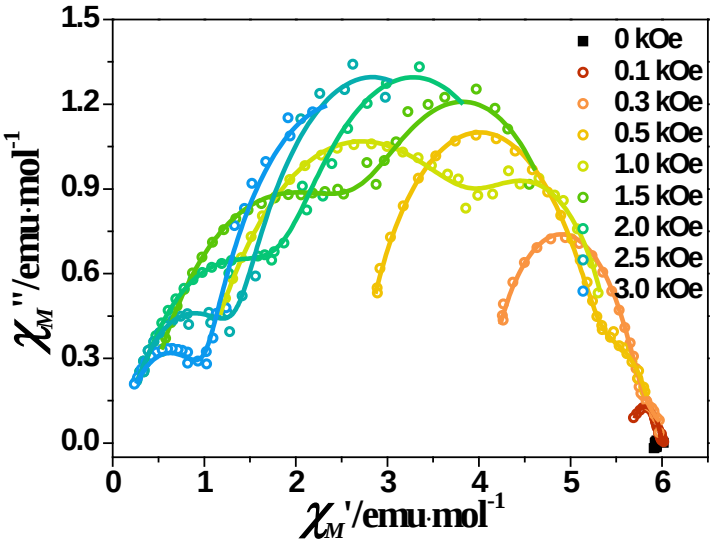

Figure S9. Cole-Cole plots of **1** in indicated *dc* fields at 2 K. The solid lines represent the simulated results.

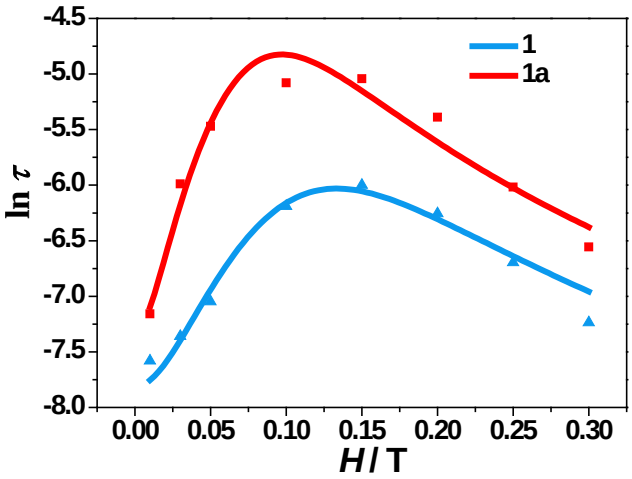

Figure S10. The ln(τ) vs. *H* plots for **1** (relaxation A) and **1a**, the solid lines represent the fitting with Eq(5).

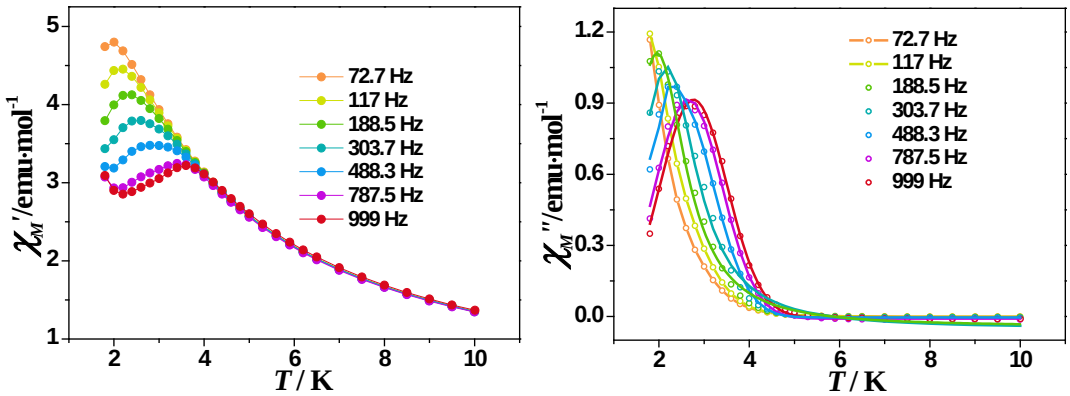

Figure S11. Temperature dependent in-phase (χ_M') and out-of-phase (χ_M") signals of **1** in 0.5 kOe *dc* field.

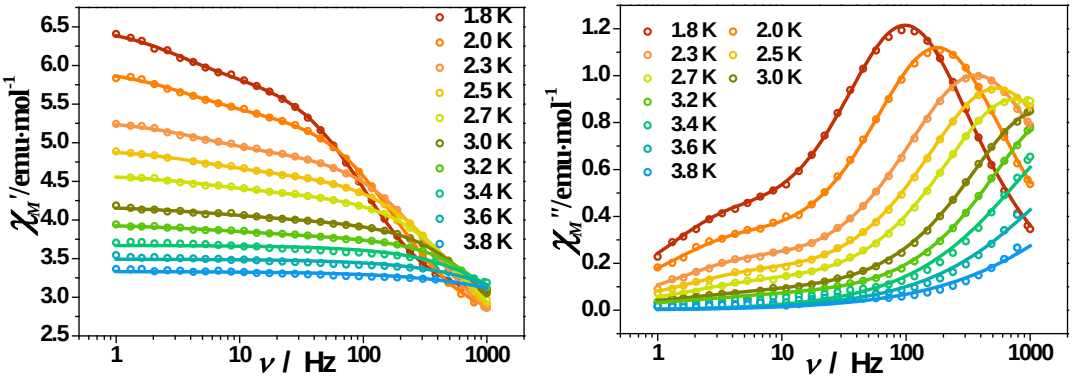

Figure S12. Frequency dependent in-phase (χ_M') and out-of-phase (χ_M") signals of **1** in 0.5 kOe *dc* field. The solid lines represent the simulated results.

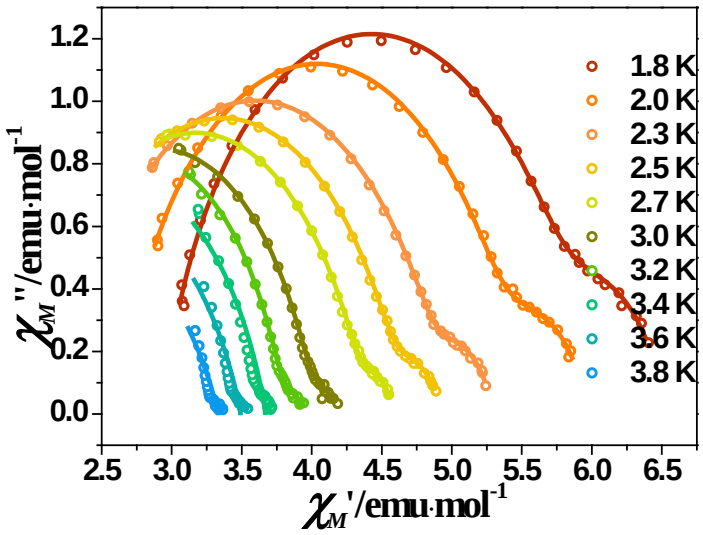

Figure S13. Cole-Cole plots of **1** in 0.5 kOe *dc* field. The solid lines represent the simulated results.

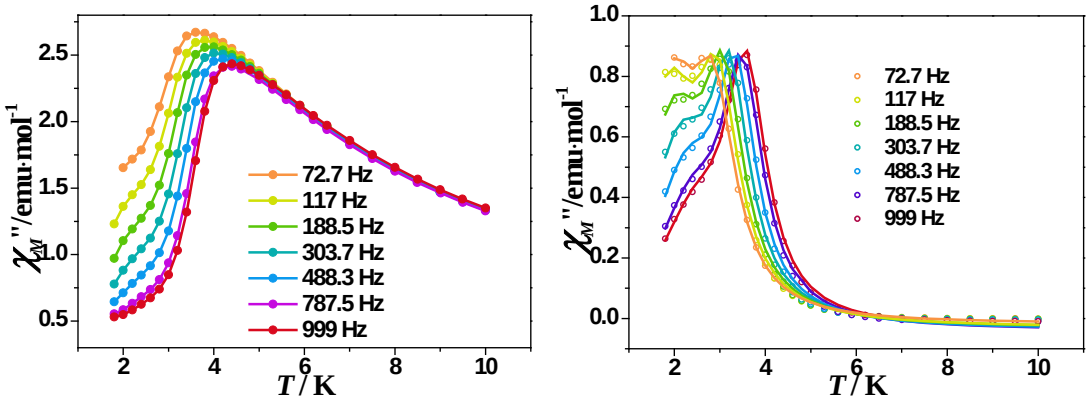

Figure S14. Temperature dependent in-phase (χ_M') and out-of-phase (χ_M") signals of **1** in 1.5 kOe *dc* field.

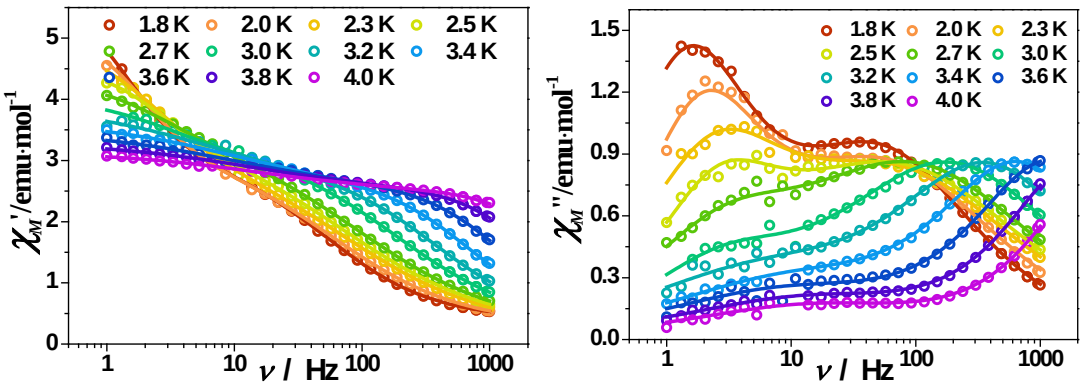

Figure S15. Frequency dependent in-phase (χ_M') and out-of-phase (χ_M") signals of **1** in 1.5 kOe *dc* field. The solid lines represent the simulated results.

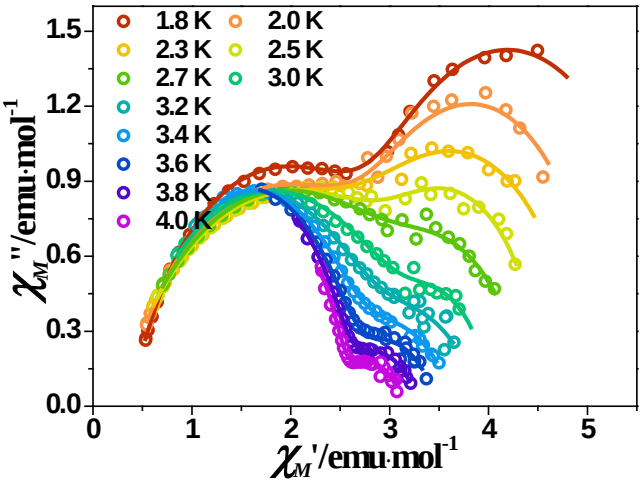

Figure S16. Cole-Cole plots of **1** in 1.5 kOe *dc* field. The solid lines represent the simulated results.

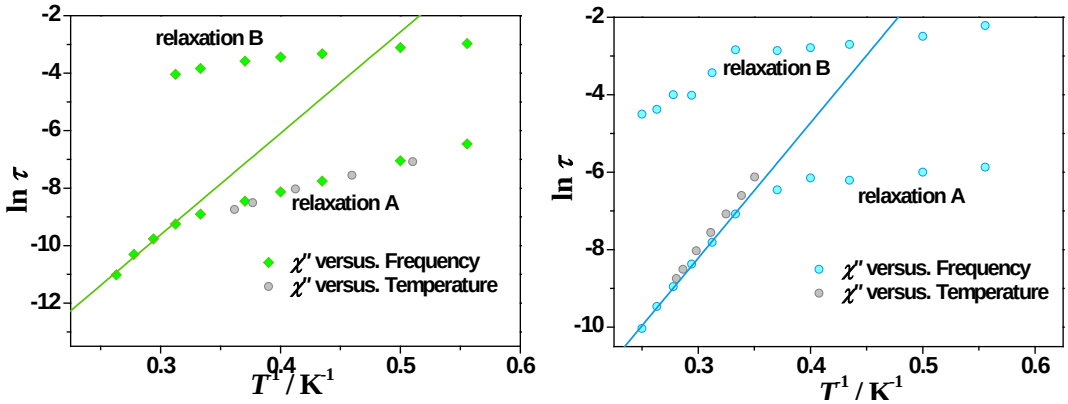

Figure S17. The ln(τ) vs. T^{-1}plots of **1** under 0.5 kOe (top) and 1.5 kOe (bottom). The solid lines represent Arrhenius fitting which yielded the anisotropy barrier: U_A = 35.3±3.2 K, τ_0 = 1.7±1.0 × 10^{-9} s for 0.5 kOe; U_A = 34.9±0.8 K, τ_0 = 7.6±1.4 × 10^{-9} s for 1.5 kOe

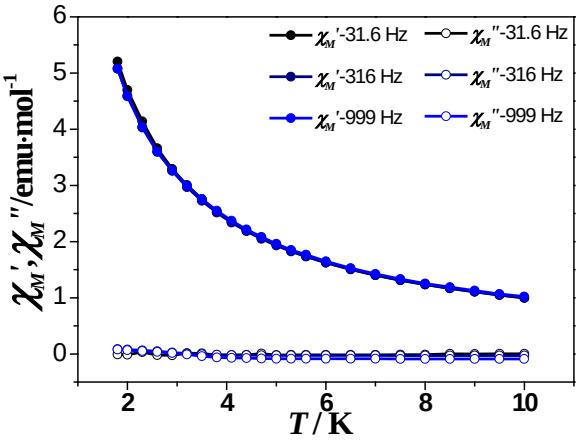

Figure S18. Temperature dependent in-phase (χ_M') and out-of-phase (χ_M") signals of **1a** in zero *dc* field.

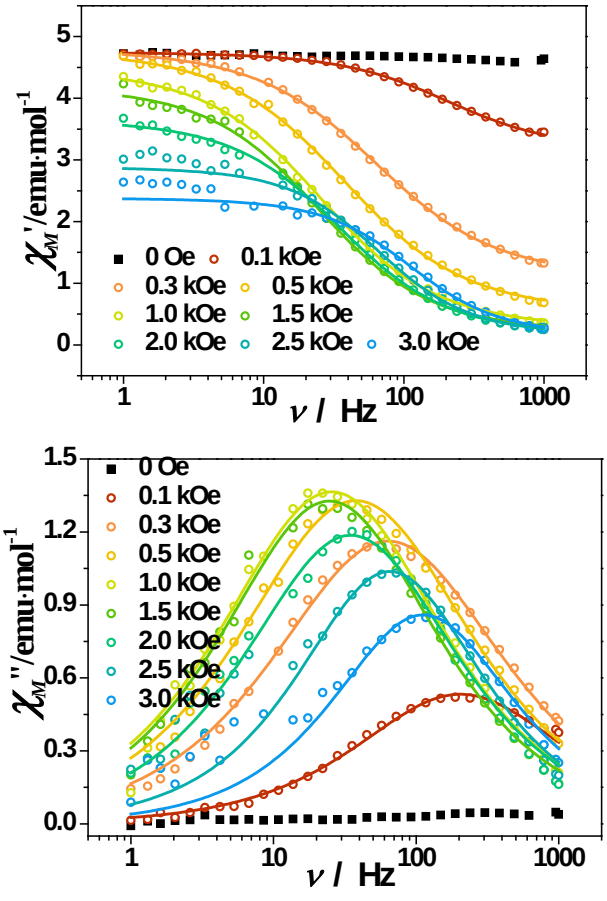

Figure S19. Frequency dependent in-phase (χ_M') and out-of-phase (χ_M") signals of **1a** in indicated *dc* fields at 2 K. The solid lines represent the simulated results.

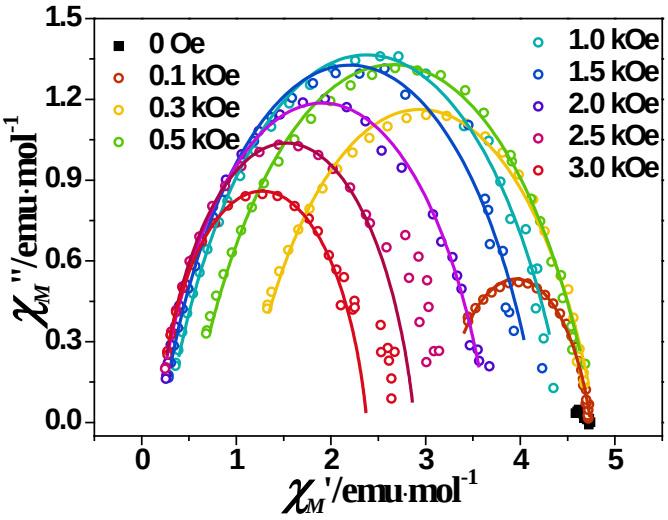

Figure S20. Cole-Cole plots of **1a** in indicated *dc* fields at 2 K. The solid lines represent the simulated results.

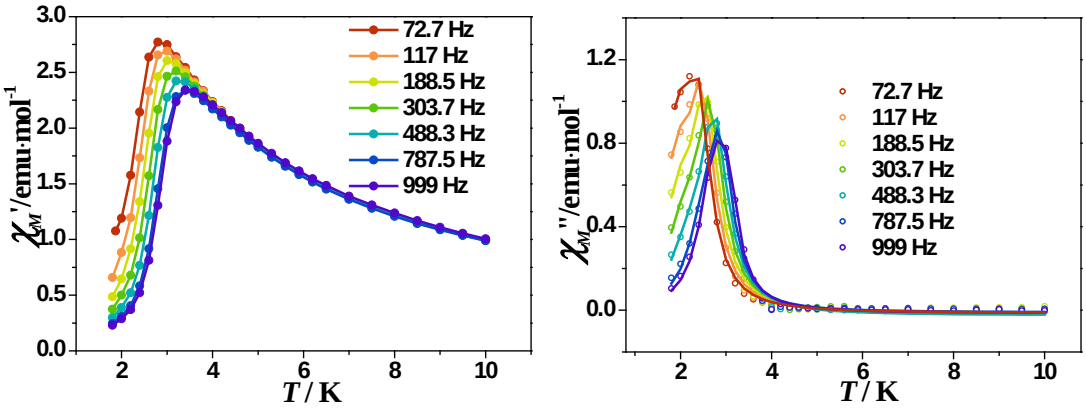

Figure S21. Temperature dependent in-phase (χ_M') and out-of-phase (χ_M") signals of **1a** in 1.5 kOe *dc* field.

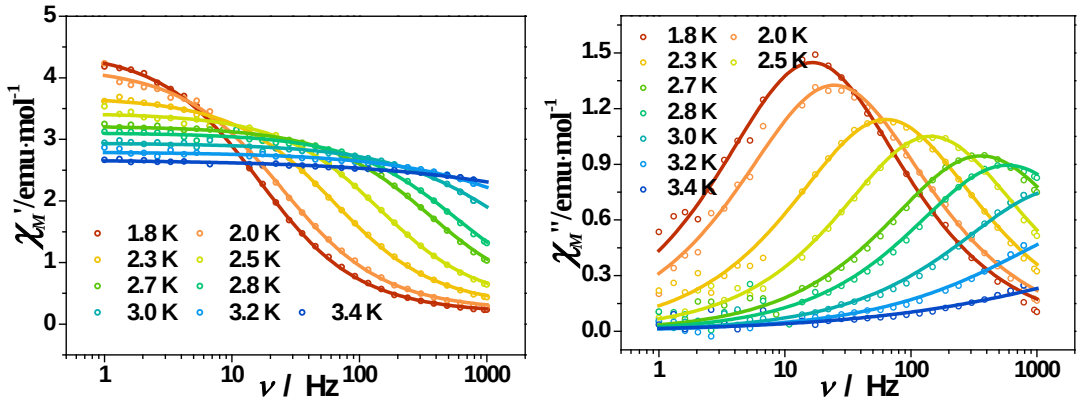

Figure S22. Frequency dependent in-phase (χ_M') and out-of-phase (χ_M") signals of **1a** in 1.5 kOe *dc* field. The solid lines represent the simulated results.

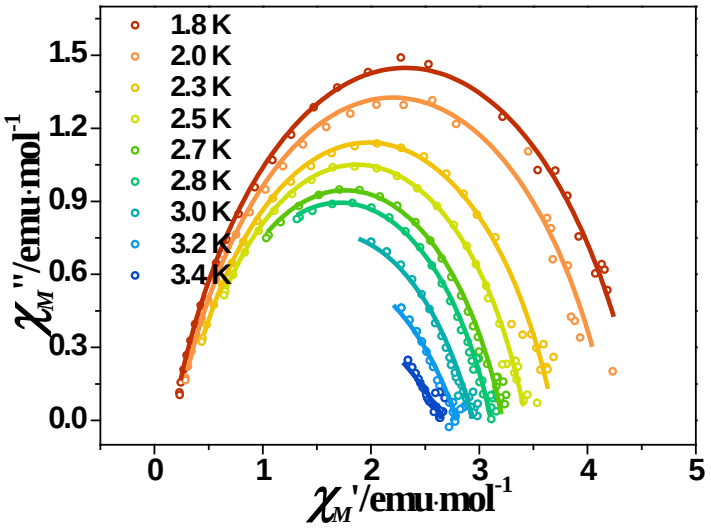

Figure S23. Cole-Cole plots of **1a** in 1.5 kOe *dc* field. The solid lines represent the simulated results.

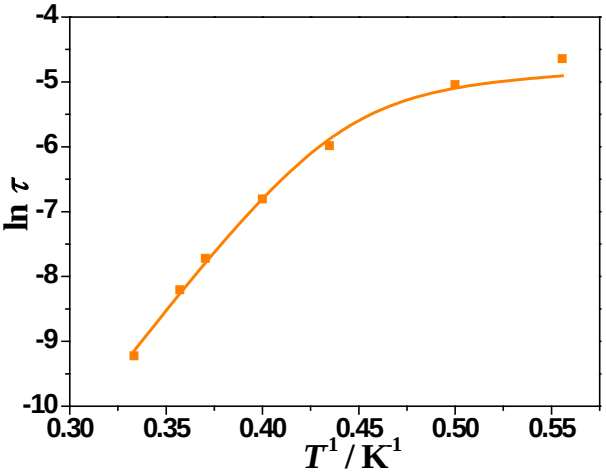

Figure S24. The ln(τ) vs. T plot for **1a**. The solid line represents the best fitting with Eq(6).

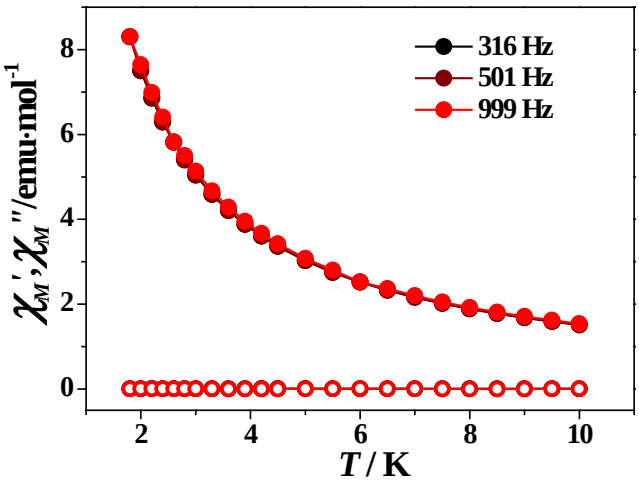

Figure S25. Temperature dependent in-phase (χ_M') and out-of-phase (χ_M") signals of **2** in zero *dc* field.

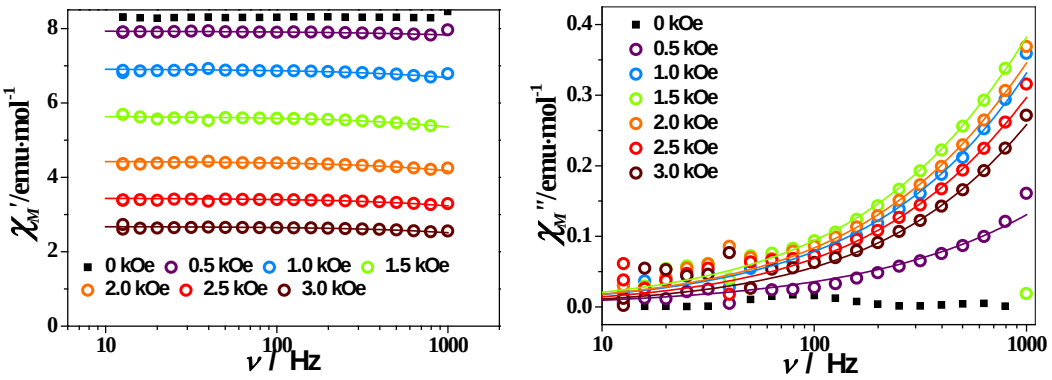

Figure S26. Frequency dependent in-phase (χ_M') and out-of-phase (χ_M") signals of **2** in indicated *dc* fields at 1.8 K.

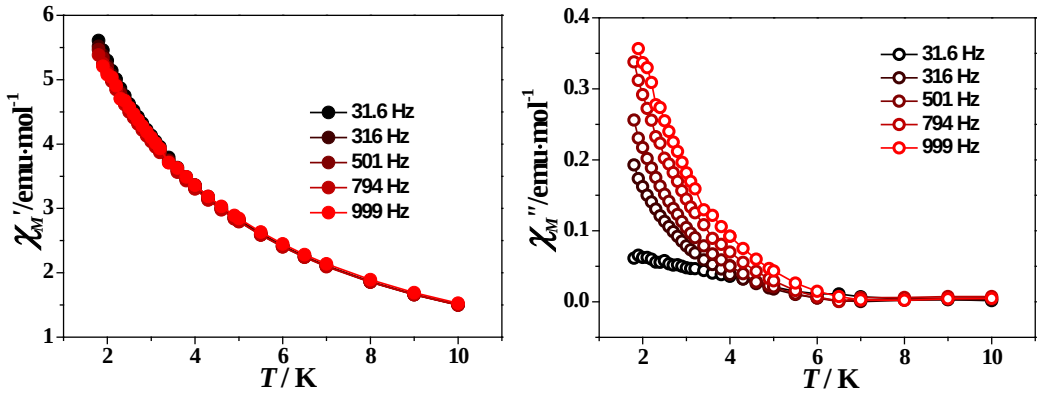

Figure S27. Temperature dependent in-phase (χ_M') and out-of-phase (χ_M") signals of **2** in 1.5 kOe *dc* field.

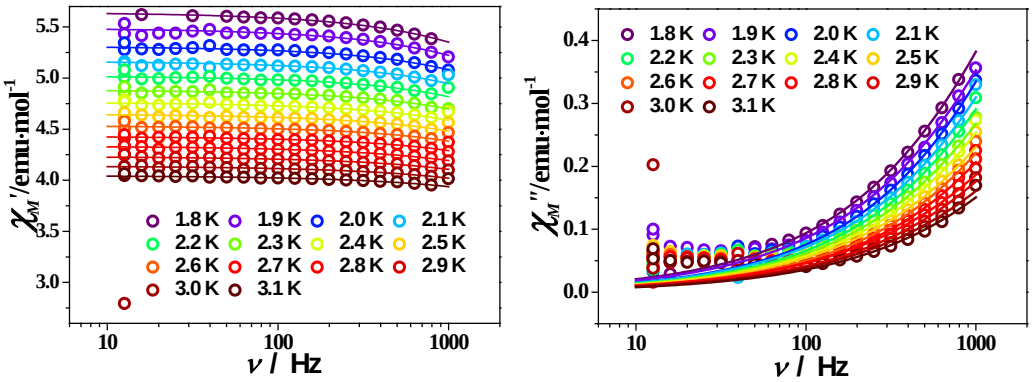

Figure S28. Frequency dependent in-phase (χ_M') and out-of-phase (χ_M") signals of **2** in 1.5 kOe *dc* field. The solid lines represent the simulated results.

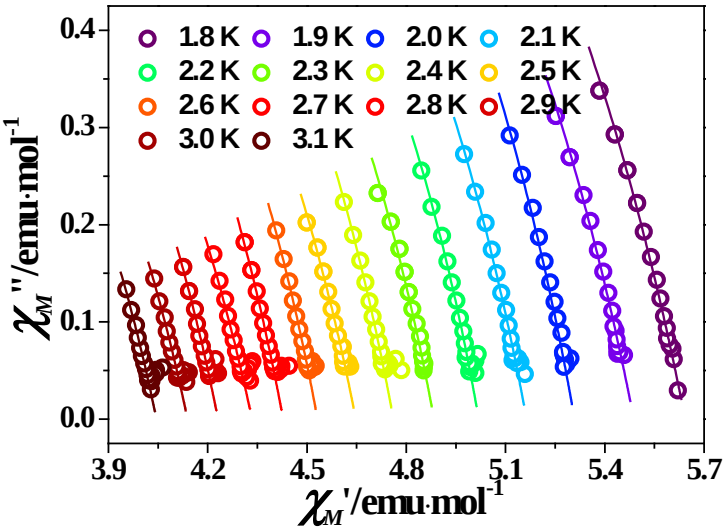

Figure S29. Cole-Cole plots of **2** in 1.5 kOe *dc* field. The solid lines represent the simulated results.

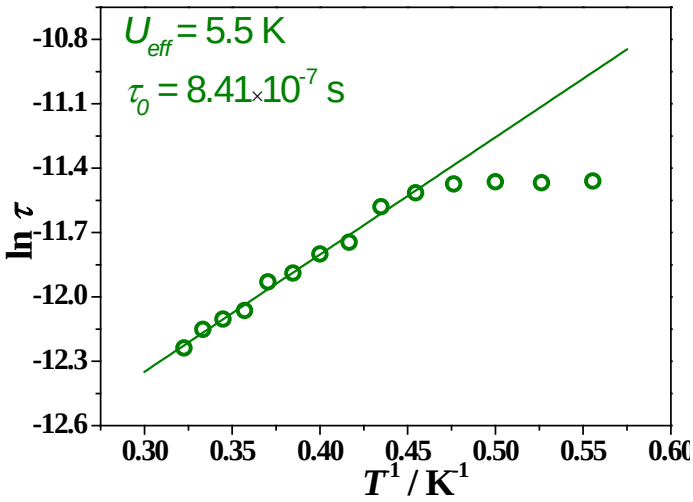

Figure S30. The logarithmic magnetization relaxation time (τ) versus T^{-1} plots with Arrhenius fitting for **2**.

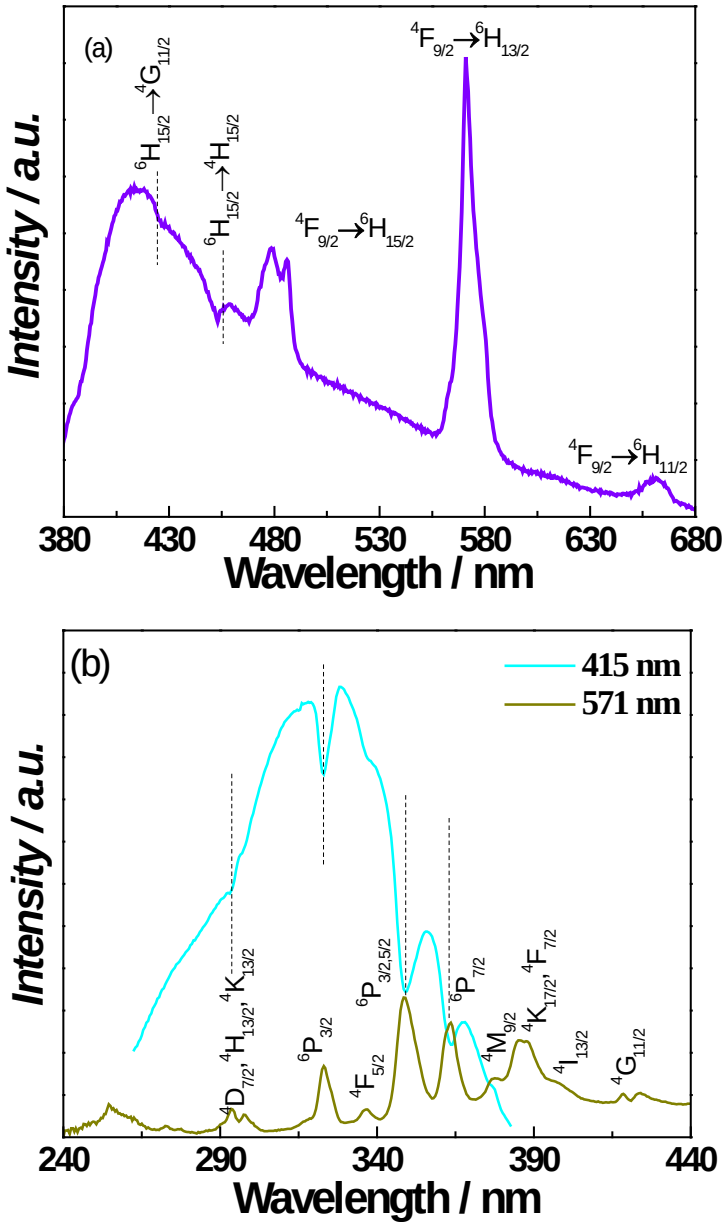

Figure S31. Room-temperature (a) emission and (b) excitation spectra of **1** excited at 349 nm and monitored at 415 nm and 571 nm, respectively. The vertical lines assign intra-4f self-absorptions.

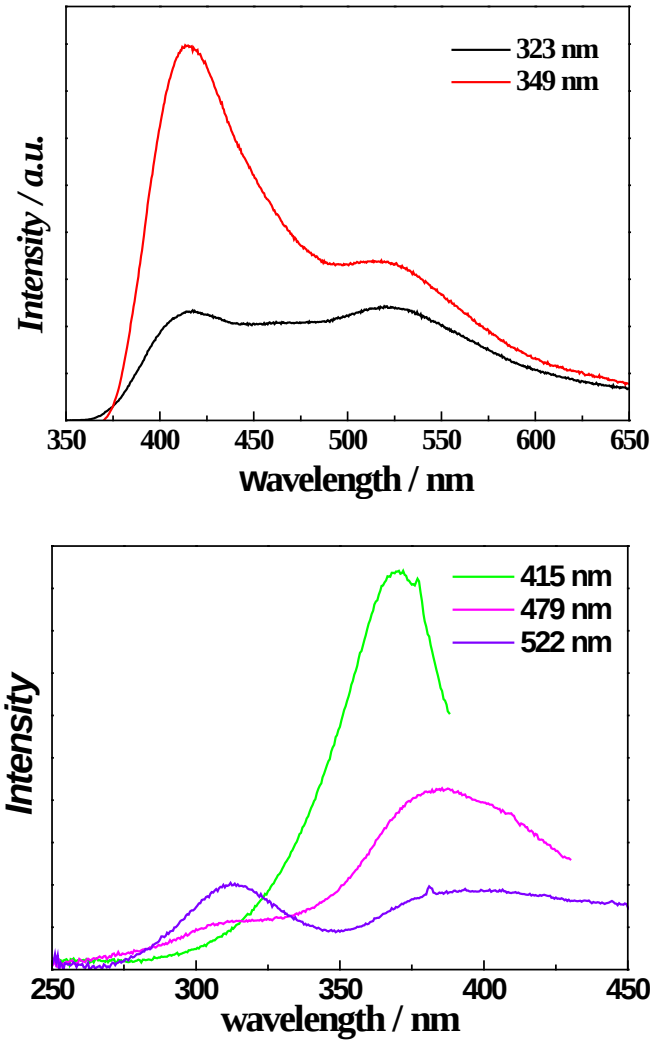

Figure S32. Room-temperature (a) emission and (b) excitation spectra of notpH_6 ligand.

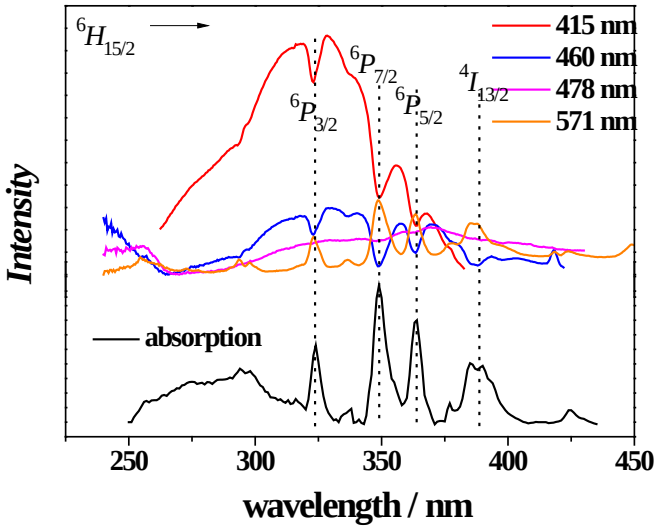

Figure S33. The excitation spectra of **1** at room temperature compared to its UV-Visible absorption spectrum.

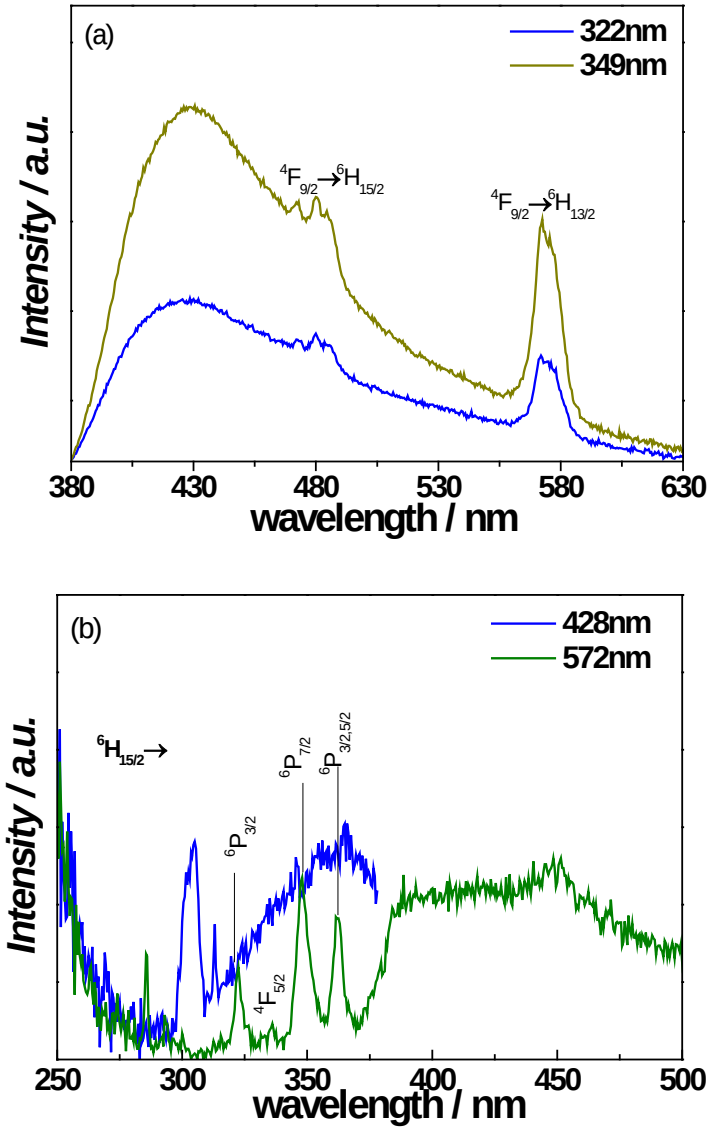

Figure S34. Room-temperature (a) emission and (b) excitation spectra of **1a** excited at 322 and 349 nm and monitored at X nm, respectively.

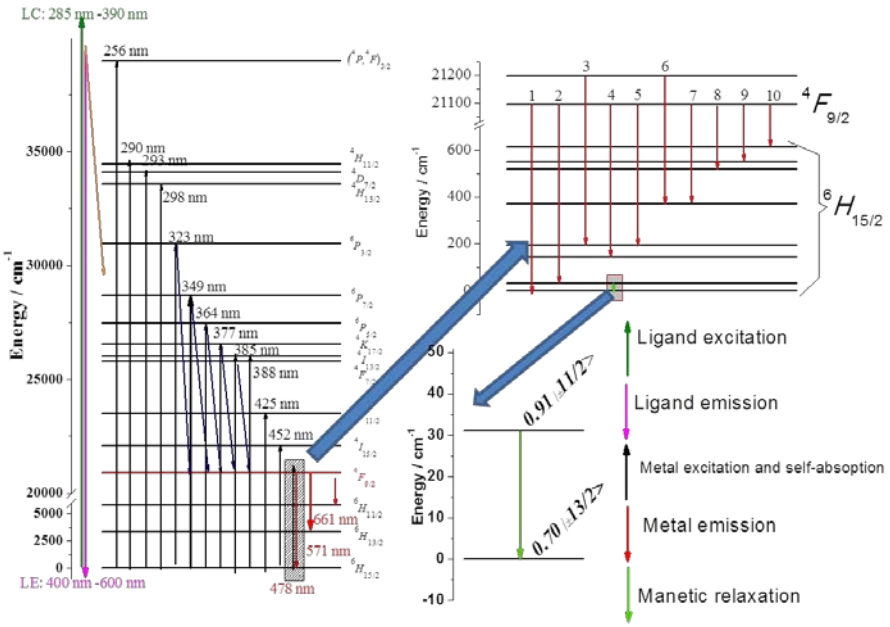

Figure S35. Energy level scheme with ligand emission, Dy^{3+} emission and self-absorption and magnetic relaxation of **1**.

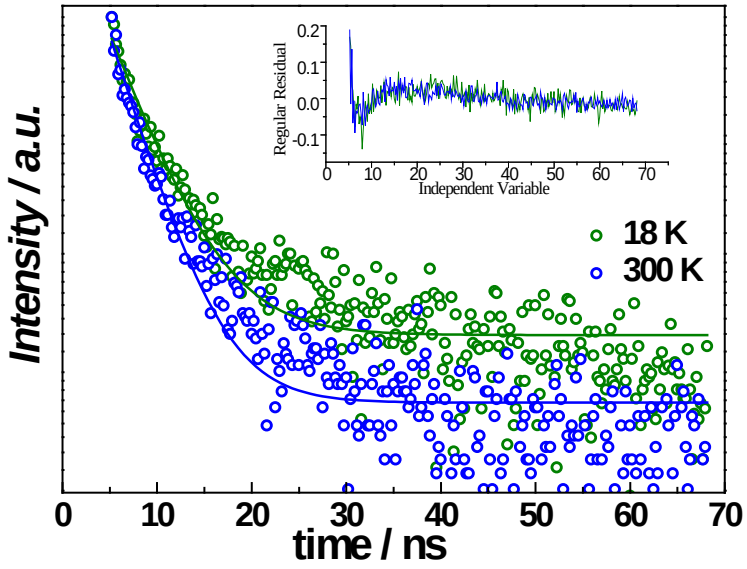

Figure S36. Emission decay curves (18 and 300K) of **1** monitored at 571 nm and excited at 355 nm. The solid lines represent the data best fit using a single exponential function. The inset shows the respective regular residual plots ($\chi^2_{red} = 1.02\times10^{-3}$, 18 K, and $\chi^2_{red} = 7.15\times10^{-4}$, 300 K) values for a better judgment of the fits quality.

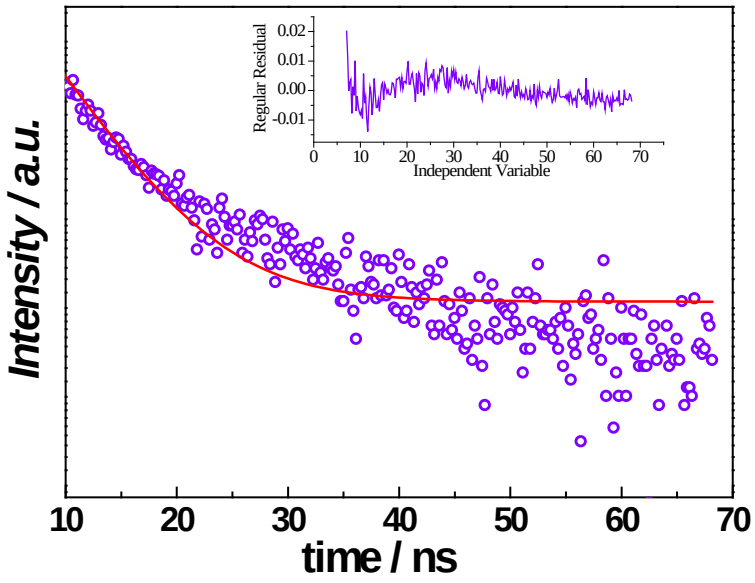

Figure S37. Room-temperature emission decay curve of **1a** monitored at 571 nm and excited at 355 nm. The solid line represents the data best fit using a single exponential function. The inset shows the respective regular residual plot (χ^2_{red}=1.62×10^{-5}) for a better judgment of the fit quality.

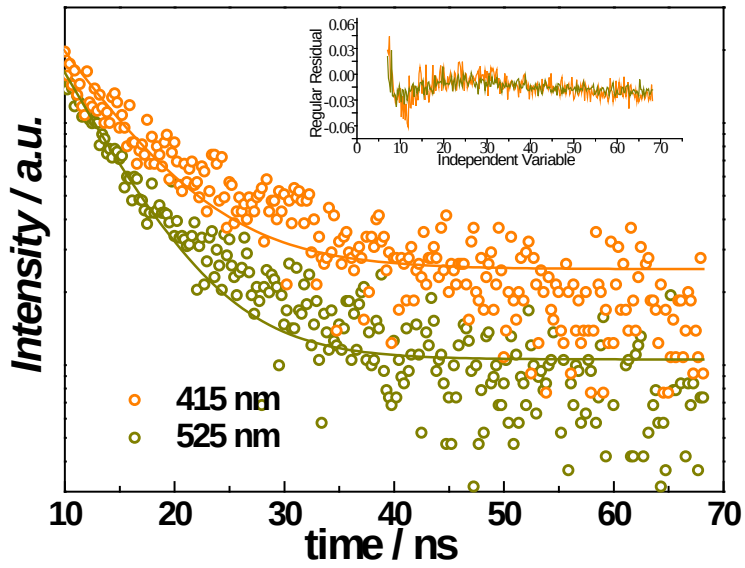

Figure S38. Emission decay curves of notpH$_6$ monitored at 415 nm and 525 nm and excited at 355 nm. The solid lines represent the data best fit using a single exponential function. The inset shows the respective regular residual plots (χ^2_{red}=1.80×10^{-4}, 415 nm, χ^2_{red}=1.80×10^{-4}, 525 nm) values for a better judgment of the fits quality.

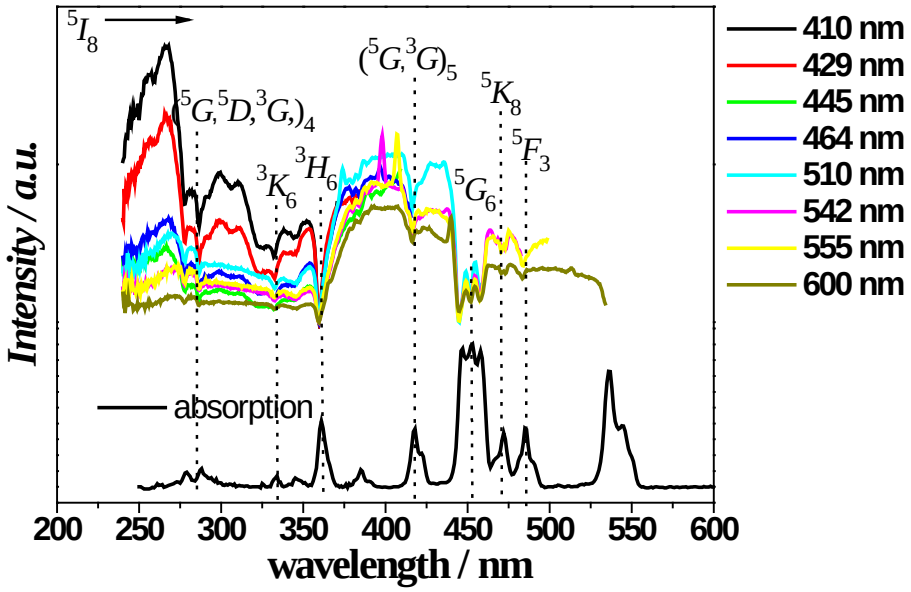

Figure S39. Room-temperature excitation spectra monitored within 410-600 nm and UV-Visible reflectance spectra of **2**.

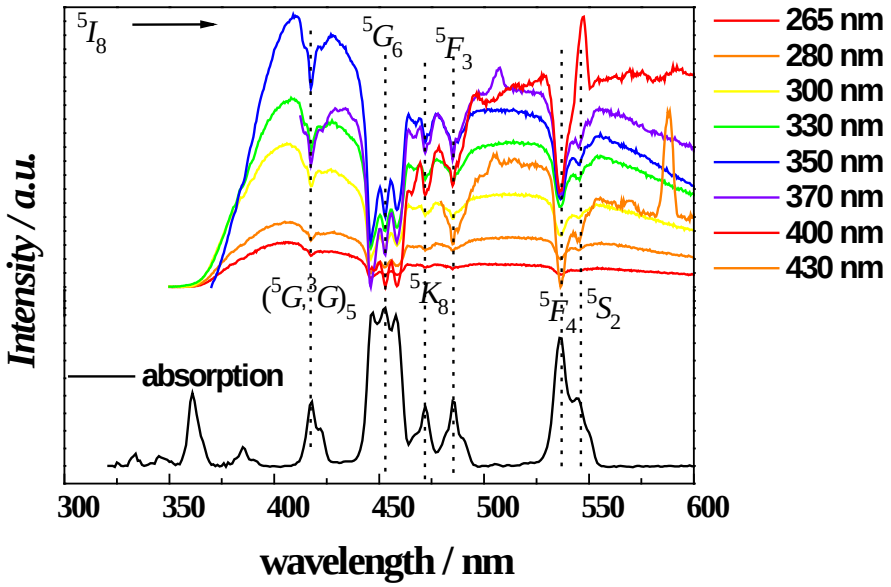

Figure S40. Room-temperature emission spectra excited between 265 nm and 430 nm and UV-Visible reflectance spectra of **2**.